



Theory of impedance for initial corrosion of metals under a thin electrolyte layer: a coupled charge transfer-diffusion model

MAIBAM BIRLA SINGH^{a,*} , B INFANT GABRIEL^{b,c}, MURALI S VENKATRAMAN^d,
IVAN S COLE^e, C GANESA MOORTHY^f and B EMMANUEL^g

^aDepartment of Chemistry, National Institute of Technology (NIT) Manipur, Imphal 795004, India

^bDepartment of Chemical Engineering, University of Washington, Seattle, WA 98195, USA

^cInstitute for Frontier Materials, Deakin University, Melbourne, Australia

^dData Analytics and AI, Energy, Water and Food, NEOM, Riyadh, Saudi Arabia

^eAdvanced Manufacturing and Fabrication Research & Innovation, RMIT University Melbourne, Victoria 3000, Australia

^fAlagappa University, Karaikudi, Tamilnadu, India

^gInstitute of Mathematical Sciences, Chennai 600113, India

E-mail: birla_26@yahoo.co.in

MS received 9 August 2021; revised 26 November 2021; accepted 29 November 2021

Abstract. An impedance model for a metal surface corroding under a thin electrolyte layer is presented. The model describes the oxygen diffusion in the electrolyte, the cathodic current via the oxygen reduction reaction (ORR) reaction and the anodic current via metal dissolution reaction (MDR) at the metal/electrolyte interface under the pseudo-steady approximation. The results for the impedance are obtained in terms of the thickness of electrolyte, the diffusion coefficient of oxygen, the concentration of dissolved oxygen and the anodic/cathodic reaction rates. The impedance characteristic are analysed through Bode and Nyquist plots which unveils six distinctive frequency regimes *viz.*, (i) purely oxygen diffusion controlled regime, (ii) electrolyte film thickness controlled regime, (iii) activation controlled regime, (iv) mixed diffusion-kinetic controlled regime, (v) capacitive electric double layer controlled regime and (vi) solution Ohmic controlled regime. The impedance response shows two asymmetrical depressed arc on the Nyquist plots indicating the Faradaic charge transfer controlled regime and purely electrolyte thickness diffusion controlled regime with an intervening straight Warburg line. The arc at low frequencies is strongly dependent on the concentration and diffusion coefficient of dissolved oxygen indicative of pseudo-steady state behaviour of interface whereas the high frequency arc represents Faradaic regimes due to MDR and ORR which is indicative of the dynamic nature of corrosion reaction rates at the interface. At thick electrolyte layer, the interface shows a mass transport controlled kinetic regime with a finite length Warburg type impedance whereas at thin electrolyte layer the interface is activation controlled with a finite diffusion Randles type impedance response. A comparison of the model with the experimental data of corroding metal shows reasonable agreement.

Keywords. Impedance; Oxygen diffusion; Corrosion; Thin films; Finite length Warburg type; Randles type; Pseudo-steady state.

List of Symbols

ω	Frequency	$Z_{\text{FLW}}(\omega)$	Finite length Warburg impedance
ω_{D}	Characteristic diffusion frequency	R_{Ω}	Resistance of electrolyte
ω_{C}	Characteristic Faradaic frequency	R_{ct}	Charge transfer resistance
$\alpha_{\text{O}_2/\text{OH}^-}$	Transfer coefficient of ORR	C_{dl}	Capacitance of EDL
$\alpha_{\text{M}/\text{M}^{\text{I}+}}$	Transfer coefficient of MDR	D	Diffusion constant of species
ΔC	Deviation of oxygen concentration from steady state concentration C_{st}	T	Temperature in Kelvin
F	Faraday's constant	Φ	Phase of impedance
		E	Potential
		$E^0_{\text{M}/\text{M}^{\text{I}+}}$	Reduction potential of MDR

*For correspondence

Supplementary Information: The online version contains supplementary material available at <https://doi.org/10.1007/s12039-021-02025-x>.

E_{O_2/OH^-}^0	Reduction potential of ORR
R	Universal gas constant
$Z'(\omega)$	Real component of impedance
$Z''(\omega)$	Imaginary component of impedance
$ Z(\omega) $	Magnitude of impedance

1. Introduction

Corrosion is a complex electrochemical multiscale and multiphysics process that takes place at metal-electrolyte interface.^{1–8} It depends strongly on the microclimatic factors like wet/dry conditions (temperature, humidity or airing), microstructure of the underlying metal,^{7,8} the thickness and composition of electrolyte (consisting of dissolved sulphates (Na_2SO_4) and chlorides (NaCl)) in contact with the metal,^{7–19} and pH.^{16–18}

Under atmospheric conditions a metal may come in contact with an electrolyte (formed by condensation of moisture) either as a droplet or thin film and react with the dissolved oxygen in the presence of salts resulting in gradual destruction of the material.^{7,8} Generally, the interaction between the metal surface and atmospheric conditions defines the thickness and the composition of the electrolyte layer in contact. The component of the atmosphere which influence the corrosion process in a thin electrolyte are mainly oxygen, water and atmospheric pollutants like SO_2 and NO . Also, the kinetics of corrosion reaction is largely affected by a combined interaction of electrolyte thickness and the individual electrode reaction. Since oxygen reduction reaction (ORR) is a dominating cathodic reaction during the corrosion process, the dependence of the corrosion rate on the oxygen is very important to understanding of the corrosion mechanism. Usually ORR associated with atmospheric corrosion is controlled by the dissolution rate of oxygen from the air and the mass-transport of the dissolved oxygen gas from the electrolyte/air interface towards the electrode surface. These are the critical factor affecting the rate of ORR. However the mass-transport in turn depends greatly on the thickness and size of electrolyte layer (aerosols) in contact with the metal surface, the electrode geometry and amount of dissolve salts. To understand the effect of electrolyte layer thickness on corrosion of metal in contact with the electrolyte, Tomashov proposed an empirical model describing the process of atmospheric corrosion in thin electrolytic film. The process of atmospheric corrosion according to Tomashov⁹ may occur in four different situations depending on the thickness of electrolyte layer L in contact:

- *Dry atmospheric corrosion* ($L < 10$ nm) - corrosion proceeds at negligibly small rates
- *Moist atmospheric corrosion* ($10 \text{ nm} \leq L < 1 \mu\text{m}$) - corrosion is anodically controlled inhibited further by the reduction of thickness with passivation and lack of water molecules for hydration of dissolved metal ions
- *Wet atmospheric corrosion* ($1 \mu\text{m} \leq L \leq 1 \text{ mm}$) - controlled by cathodic process i.e., the diffusion of oxygen in the electrolyte layer
- *Complete immersion* ($L > 1 \text{ mm}$) - corrosion rate shows a maximum when transitioning from moist (anodic control) to wet (cathodic control) conditions.¹⁸ This maximum was found to be different for different physical conditions.

Although the Tomashov's model is a widely accepted conceptual empirical model for atmospheric corrosion which indicate the dependence of corrosion rate on the thickness of electrolyte layer, it lacked the quantitative and the mechanistic description of the relationship between the electrochemical kinetics and the film thickness. However an interesting feature of the model is the anticipation of a critical electrolyte film thickness, positing a transition from a plateau in corrosion rate when a constant diffusion layer was attained to cathodically controlled corrosion limited diffusion of the dissolved oxygen to the reaction surface.⁹ The corrosion rate increases as the film thickness decreases under the so-called "critical thickness" and further transition into reduced (anodic controlled) due to lower solubility of corrosion product in smaller volume. Finally, for very thin electrolyte thickness, the corrosion proceeds at very low rates.

There has been experimental studies to understand the transition from bulk, fully immersion kinetics to thin film kinetics.¹² However, different workers have reported different values of critical thickness. For e.g., Nishikata *et al.*,^{14–16} reported that the critical electrolyte film thickness exist in the vicinity of 1 mm. Similarly experimental works by Stratmann *et al.*,^{10–12} and Frankel *et al.*,²⁰ corroborate the presence of critical electrolyte film thickness between 500 μm to 1 mm. The exact value of critical thickness is still not clear. It is suggested that the critical value denotes the minimum thickness at which boundary layer established by natural convection dictates mass transport.^{21, 22} A proper quantification of the corrosion rates with respect to various factors influencing corrosion under a thin electrolyte film is required to advance our understanding.

In general, corrosion is an electrochemical process and the process of corrosion may be studied employing electrochemical techniques. The experimental studies to understand the corrosion under a droplet or in contact with a thin electrolyte layer of pure metal (like iron,^{10–16,23} magnesium,²⁴ copper,^{25,26}) and alloys (like Al-Mg,²⁶ Al-Zn,^{27,28} etc.) have been made using Kelvin probe,^{10–16,23} electrochemical impedance spectroscopy (EIS),^{14–16,23,25} polarization,^{25,29} electrochemical noise,³⁰ or a combination of methods.^{31,32} Studies have been made to have analyzed corrosion reaction under mixed transfer-diffusion control for potentiostatic current transient, and under constant current conditions.^{33,34} However, the presence of extremely thin electrolyte makes it is difficult for conventional electrochemical techniques employing Luggin probes to obtain a uniform current and the solution resistance is very high^{14,35}. Thus a severe limitation of the conventional steady-state techniques comes from the electrolyte resistance located between the equipotential surface defined by the reference electrode and the working electrode. In such conditions due to an extremely high ohmic drop and a non-uniform current (potential) distribution over a working electrode produces serious errors in the measurement of the atmospheric corrosion rate and Faradiac process. It is difficult to obtain accurate results of the corrosion processes at large ohmic drop compared with Faradaic overvoltage due to reaction. The potentiostatic modes are affected and the ohmic drop in thin electrolyte layer can introduce considerable error in electrochemical polarization measurements and hence the current (galvanostatic) techniques may be incorrect in extracting the electrochemical quantities like polarization resistance and ohmic resistance. Furthermore, accurate in-situ corrosion rate monitoring, i.e. without errors due to inhomogeneous current distribution, can be done even during the drying process when only a very thin layer of water is present on the specimen surface.³⁵ Owing to complex nature of atmospheric corrosion, studies focussing on experimentally understanding the mechanism and the rates of ORR and also oxygen diffusion as a function of the thickness of electrolyte film employing a single electrochemical technique is not encourage. Since each electrochemical technique has advantages and limitations, often a synergistic use of various techniques is desirable to obtain a meaningful result. A combination of experimental data (obtained through a synergistic correlation of various experimental techniques) with mathematical corrosion model should be a solution to understand

the complex process of (atmospheric) corrosion. To this end, multiscale modelling approaches,^{2–4,36} to integrate various complex processes involved in atmospheric corrosion is proposed to bridge the gap between electrochemical quantification and outcome of corrosion experiments.

There has been theoretical modelling of the corrosion of metal under a thin electrolyte,^{36–45} for various situations. The recent developments in the research of atmospheric corrosion for thin electrolyte films and droplets have been summarized in the reviews by Simillion *et al.*,⁴ and Koushik *et al.*⁴⁶ A recent perspective by Sadikhani and Blackwood,⁴⁷ highlights the importance of finite element methods for thin film corrosion modelling and the need for dynamic electrolyte thickness modelling in conjunction with moving boundary modelling. Also Cole,⁴⁸ have reviewed the progress in atmospheric corrosion of galvanised steel and zinc and emphasised on the need to include multi-layered structures and compact layer structures in oxide layer formed, its role in ORR in corrosion modelling of porous oxide under the thin electrolyte layer. Further, it was stressed that semi-conducting nature of the oxide and the defects are important factors that controls the growth and dissolutions of oxides.⁴⁸

We also have advanced a model for free corrosion of the metal under a thin electrolyte film under pseudo-steady state diffusion of oxygen in the electrolyte layer where the anodic metal dissolution reaction (MDR) and cathodic oxygen reduction reaction (ORR) densities balance to provide a zero net current density at the metal surface.^{37–41} Our model presented a non-linear dependence of dissolved oxygen concentration at the metal surface with the corrosion current density and predicted the corrosion potential by establishing “thin-electrolyte layer” (mass-transfer) corrections to the mixed-potential theory. Similar models for the corrosion under a thin electrolyte layer have been developed employing the numerical multi-ion transport and reaction models to understand the influence of electrolyte film thickness, dissolved salt (NaCl) concentration and geometry on the oxygen reduction current.^{42,43} However, to best of our knowledge, no theoretical model of corrosion under a thin electrolyte layer has been able to explain the Tomashov’s empirical model.

Here, in this work, we develop an impedance based model including both charge transfer and mass transport effect as an alternative to our current based model,^{37–41} employing the basic model framework,³⁹ for the impedance of corrosion of metal under a thin

film. Particularly we are interested in developing an impedance model, since ESI is non-destructive electrochemical technique that can be used to investigate bulk as well as interface process with time constants ranging from minutes down to microseconds. It can be used to investigate the electrode kinetics of a reaction in electrolyte film in corrosion studies, and double layer kinetics. In the case of a corroding interface in which, the nature of both the metal and the thickness of electrolyte solution exerts an influence on the charge transfer processes occurring there, ESI is particularly advantageous to probe the interface. This paper is organized as follows: (i) following our earlier work,³⁹ we describe the problem of corrosion of metal under a thin electrolyte layer involving a coupled dissolved oxygen diffusion limited-charge transfer process. The Faradaic process *viz.*, the MDR current density is described by the Butler-Volmer expression and ORR current density is given by the stoichiokinetic equation,^{37,49} (ii) we summarize the impedance model and its analytical solutions, (iii) we analyse the results of the model by comparing with experiments and finally establishing the conclusions of our work.

2. Impedance model for metal corrosion under a thin electrolyte layer

To develop a theory for the corrosion of metal under a thin electrolyte layer, we consider a general situation as shown in Figure 1. Four steps are recognized:^{16,37} (i) dissolution of O₂ from the air into the electrolyte layer, (ii) diffusion of O₂ through the electrolyte film, (iii) charge transfer at the metal/electrolyte interface due to ORR and MDR and finally (iv) diffusion of reaction product (OH⁻ and Mⁿ⁺) from the metal surface. At the air-electrolyte interface, the concentration of dissolved oxygen *C* is assumed to be in equilibrium with the oxygen in atmosphere *C*^{sat} (i.e., *C* = *C*^{sat}) as given by Henry's law.⁵⁰ *C*^{sat} depends on the amount of salt dissolved,⁵¹ at the given temperature and pressure. The ORR may take place by either 2e⁻ or 4e⁻ or both pathways depending on the type of metal, pH, concentration of dissolved salts, etc.⁵¹ This process occurs simultaneously with the MDR (inherently faster than ORR) leading to the formation of OH⁻. Typically oxygen diffusion is the rate-determining step in the corrosion of an active metal under a thin electrolyte film.

The two Faradaic processes *viz.*, MDR and ORR constitute the corrosion process. MDR is represented as a single step process.⁵²

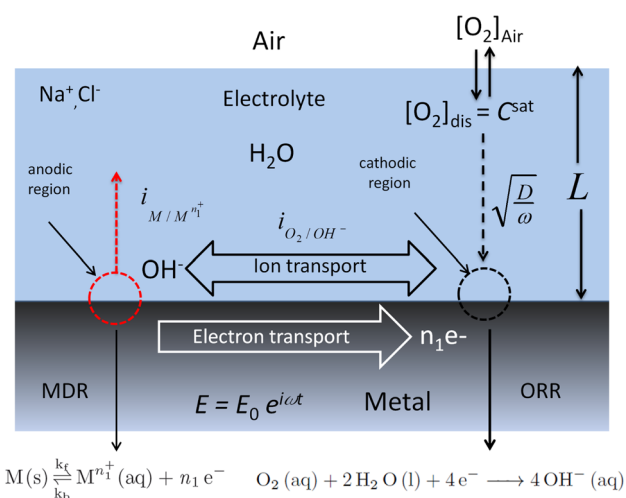
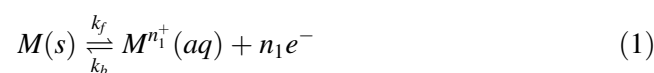
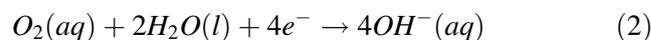


Figure 1. Schematic illustration of various process of metallic corrosion under a thin electrolyte layer of thickness *L* in presence of dissolved salts (NaCl) under an applied potential perturbation $E = E_0 e^{i\omega t}$. Here the red dotted arrow line is indicative of the anodic MDR given by equation 1, the black arrow line is indicative of cathodic ORR given by equation 2 and the corresponding current densities for MDR and ORR are $i_{M/M^{n+}}$ and i_{O_2/OH^-} respectively. The black dotted arrow line indicates the phenomenological diffusion length ($\sqrt{D/\omega}$) characteristic of the oxygen diffusion in the electrolyte layer. The electrolyte layer is assumed to be saturated with dissolved oxygen whose concentration is C^{sat} .



The reduction of oxygen may take place via two or more different pathways.⁵³ However since the functional form of ORR kinetics derived using the stoichiokinetic equation approach remains unchanged,^{37,49} we use a single representative reaction



to describe the reduction of oxygen in the thin (neutral or basic) electrolyte layer. We have developed an impedance model for initial corrosion of metals under a thin electrolyte layer in presence of electric double layer (the details of mathematical derivations are provided in supplementary information).

The total impedance density $Z(\omega)$, may be written as

$$Z(\omega) = \frac{1}{\left[\frac{1}{R_{ct}} + \frac{n_2 F C_s J_{sat}'}{(1 + \tanh(\sqrt{i\omega/\omega_i})/(\sqrt{i\omega/\omega_i})) + i\omega C_{dl}} \right]} \quad (3)$$

where R_{ct} is the charge transfer resistance and C_{dl} is the EDL capacitance. The quantity

$$\omega_i = f_{st}^2/D = \left(\frac{i_{st}}{n_2 F C_{st}} \right)^2 \frac{1}{D} \quad (4)$$

is the characteristic frequency related to the steady state current and denotes the competition of Faradaic process to that of diffusion process in the thin electrolyte film. Here, f_{st} has a dimension of m/s and defines the rate of charge transfer due to corrosion. Further the quantity

$$\omega_L = D/L^2 \quad (5)$$

is the characteristic frequency associated with diffusion and characterizes the finite thickness of electrolyte layer in the system. The second term in the denominator in r.h.s of equation 3 may be further simplified substituting the value of $f'_{st} = (i_{st} \alpha_{O_2/OH^-}) / (RT C_{st})$ (see supplementary information for more details) for steady state assuming that the perturbation in potential have small effect of exchange current density to obtained a more recognisable impedance expression as^{54,55}

$$\frac{1}{Z(\omega)} = \frac{1}{R_{ct}} + \frac{1}{R_D \left\{ 1 + \frac{\tanh(\sqrt{i\omega/\omega_L})}{(\sqrt{i\omega/\omega_i})} \right\}} + i\omega C_{dl} \quad (6)$$

where $R_D = RT / (n_2 F \alpha_{O_2/OH^-} i_{st})$ is the resistance associated with mass transport of oxygen which depends on steady state current density of ORR. Now accounting the Ohmic resistance of the electrolyte, the total impedance of thin electrolyte layer given by equation 6 may be written explicitly as

$$Z(\omega) = R_\Omega + \frac{1}{\frac{1}{R_{ct}} + \frac{1}{R_D + Z_{FLW}} + i\omega C_{dl}} \quad (7)$$

where

$$Z_{FLW} = \frac{Z_D \tanh(L\sqrt{i\omega/D})}{\sqrt{i\omega/D}} \quad (8)$$

is the finite length Warburg (FLW),^{54,55} impedance which shows the relationship between the coefficient and the thickness of the electrolyte film with impedance co-efficient

$$Z_D = \frac{RT}{n_2^2 F^2 \alpha_{O_2/OH^-} C_{st} D} = \frac{R_D}{|k_2^{-1}|} \quad (9)$$

Since $|k_2^{-1}|$ has a dimension of length and characterized the effective thickness of steady state layer where the concentration is varied, thus Z_D may be physically interpreted as diffusion resistance R_D per unit length in

the finite electrolyte layer. The finiteness of the electrolyte is associated with the impedance Z_{FLW} given by equation 8. The effect of electrolyte layer thickness on Z_{FLW} is show in the supporting information Figure S1, Supplementary Information.

2.1 Limiting cases

The limiting impedance for thin and thick electrolyte layer may be obtained from equation 7 as follows:

Case (a): For very thin electrolyte layers $L \rightarrow 0$ (corresponding to dry to moist atmospheric corrosion), the effect of mass transport is negligible and the interfacial response is kinetic controlled with impedance

$$Z(\omega) = R_\Omega + \frac{1}{\frac{1}{R_{ct}} + \frac{1}{R_D} + i\omega C_{dl}} \quad (10)$$

The impedance expression suggest a combination of two parallel impedance viz., the charge transfer impedance (R_{ct}) and diffusion layer (R_D) impedance in series with EDL capacitance and Ohmic impedance. This limit corresponds to Randles situation of Faradiac charge transfer,^{56–59} in presence of finite length diffusion. The impedance response of such situation may be identified in the Nyquist plot as a combination of an arc at high frequency and straight Warburg line at low frequency.

Case (b): For thick electrolyte layer with $L \rightarrow \infty$ (corresponding to wet to complete immersion) we have the semi-infinite diffusion limit whose impedance is given by

$$Z(\omega) = R_\Omega + \frac{1}{\frac{1}{R_{ct}} + \frac{1}{R_D(1+\sqrt{i\omega/\omega_L})} + i\omega C_{dl}} \quad (11)$$

This limit corresponds to a situation where the FLW impedance,^{54,55} results in Warburg impedance,^{60,61} and can be identified in the Nyquist plots as two arcs with an intervening Warburg line which forms a part of the (usually) larger arc at low frequency. The arc at high frequency is characterized by ω_Ω and at low frequency is characterized by ω_D . The features that arise due to the competition between the Faradaic processes and electrolyte layer thickness dependent diffusion of oxygen are characterized by two frequencies ω_i and ω_L .

Case (c): For electrolyte thickness comparable to diffusion length $L \sim L_D$ (corresponding to moist-wet conditions), at a characteristic critical diffusion frequency ω_D , the FLW impedance is described by

$$Z_{FLW} = \frac{Z_D \tanh(\sqrt{i\Lambda})}{\sqrt{i\omega/D}} \quad (12)$$

where Λ is a finite dimensionless length equal to square of the ratio of the system's finite length L to the diffusion length of the system L_D i.e. $\Lambda = (L/L_D)^2$ and Z_D is given by equation 9. The overall impedance in such cases is

$$Z(\omega) = R_\Omega + \frac{1}{\frac{1}{R_{ct}} + \frac{1}{R_D + (Z_D \tanh(\sqrt{i\Lambda})/\sqrt{i\omega/D}) + i\omega C_{dl}}} \quad (13)$$

The limiting cases (a), (b) and (c) in a corroding system arises due to the combination of MDR and diffusion limited ORR in varied finite thick electrolyte layer under various atmospheric conditions. Unlike the response of pure diffusion controlled single step redox reaction, i.e., $O + ne^- \rightleftharpoons R$ (Randles situation,^{57–59}) and the diffusion in finite thick electrolyte layer (finite length Warburg type impedance,^{54,55}) the combination of MDR and diffusion limited ORR reaction in finite electrolyte layer in contact with metal surface give rise to a variety of coupled features (see results and discussion)^{33,34,62} not observed in earlier models.

3. Results and Discussions

In this section we first discuss the various impedance characteristic frequencies pertaining to our impedance model equation 7. We also compare various limiting cases to provide physical significance of the associated situation in corrosion of metal under a thin electrolyte layer. Further we discuss the dependence of electrochemical impedance on electrolyte thickness, diffusivity of oxygen and change in anodic/cathodic rates. Finally, we compare the prediction of our theoretical impedance model with the experimental corrosion data.

3.1 Impedance characteristics and phenomenological frequencies

An important quantity that may be obtained from ESI is the time scale of impedance response which characterized the associated electrochemical phenomena. Figure 2 show the graphical illustration of qualitative impedance characteristic (six regimes) and the possible five phenomenological characteristic frequencies associated with our impedance model equation 7 pertaining to the corrosion of metal under a thin

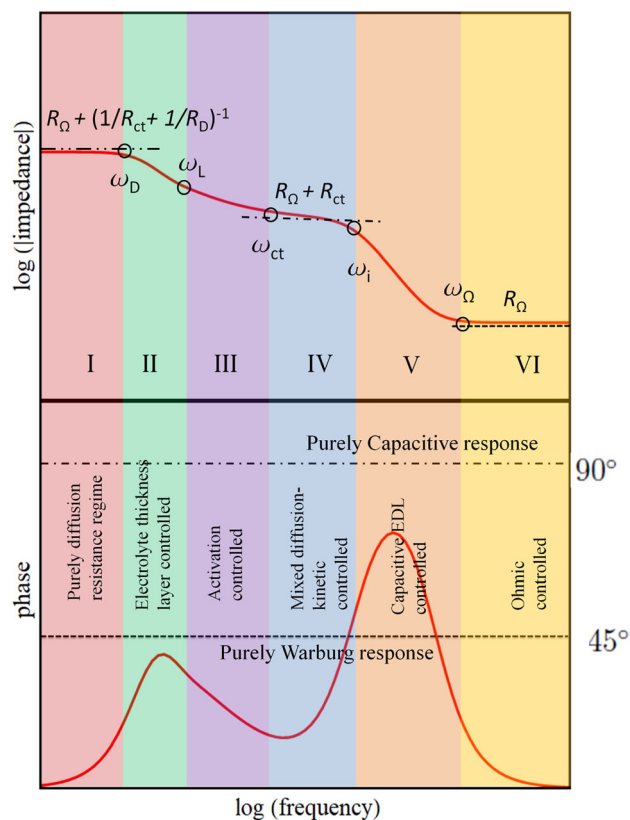


Figure 2. Schematic illustration of impedance characteristics indicating the various phenomenological frequencies and their associated regimes in Bode plot representation. The upper panel shows the log (impedance) vs. log (frequency) plot and the lower panel shows the phase vs log (frequency) plot.

electrolyte. The six regimes (see Figure 2) are identified as (i) purely diffusion resistance controlled regime (I), electrolyte layer thickness regime (II), activation controlled regime (III), mixed diffusion-kinetic controlled regime (IV), capacitive EDL controlled regime (V) and Ohmic controlled regime (VI). The associated characteristic frequencies associated with these six regimes are *viz.*, (i) diffusion layer frequency $\omega_D = D/L_D^2$, which characterizes the diffusion time scales, (ii) finite electrolyte layer frequency $\omega_L = D/L^2$, which characterizes the diffusion of dissolved oxygen in the finite thickness electrolyte layer L , (iii) charge transfer relaxation frequency $\omega_{ct} = (R_{ct}C_{dl})^{-1}$, which characterizes the time of relaxation of coupling of the MDR and the EDL capacitance, (iv) frequency depending on corrosion current $\omega_i = \left(\frac{i_{st}}{n_2FC_{st}}\right)^2 \frac{1}{D}$ which describes the relaxation time of ORR current flowing in the diffusion layer at steady state and (v) the electrolyte layer bulk relaxation frequency $\omega_\Omega = (R_\Omega C_{dl})^{-1}$ also called the Ohmic relaxation frequency which describes the time

scale of relaxation of the bulk couple with the EDL capacitance.

The impedance characteristic of the six regimes are as follows :

- (1) At very low frequencies $\omega < \omega_D$, we observe the purely diffusion resistance controlled regime (I in Figure 2) where the magnitude of the slope of $\log |Z|$ vs $\log \omega$ plot is zero and we have an impedance plateau with

$$Z(\omega < \omega_D) = R_\Omega + \left(\frac{1}{R_{ct}} + \frac{1}{R_D(1 + \sqrt{\omega_i/\omega_L})} \right)^{-1} \quad (14)$$

Correspondingly the phase plots (lower panel) in Figure 2 shows the phase is less than 45° and tends to zero in the plateau region of impedance.

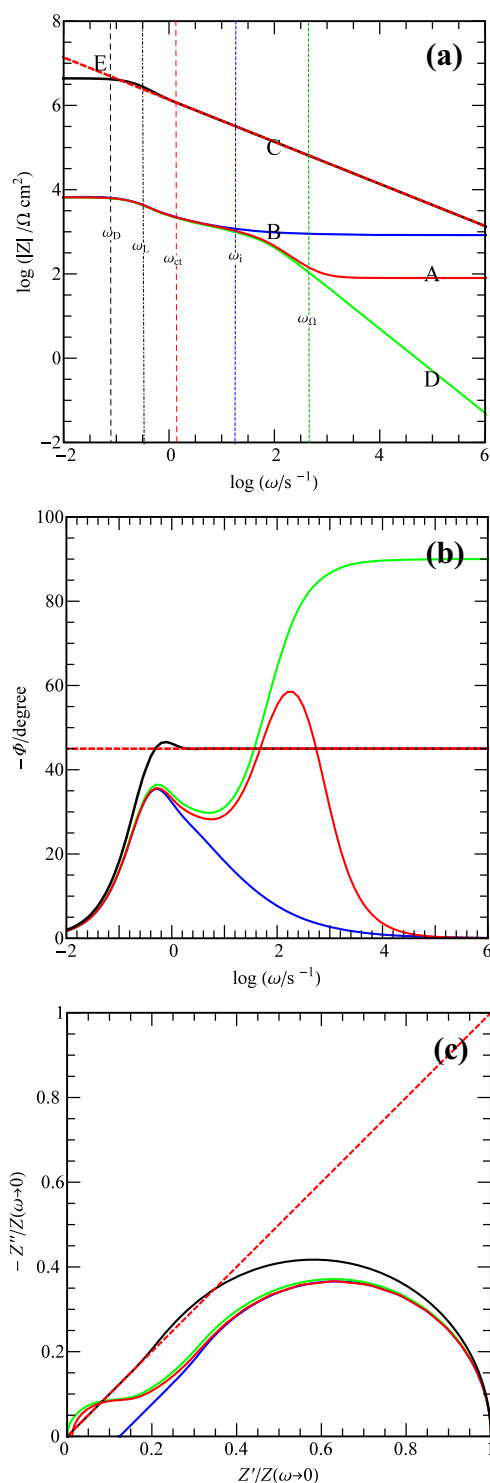
- (2) At frequencies in the range $\omega_D < \omega < \omega_L$, we see the onset of electrolyte thickness dependent diffusion regimes (II) where the slope $\log |Z|$ vs $\log \omega$ is less than $(1/2)$. Here the phase increase from 0° towards pure Warburg value of 45° but less than 45° . The phase value satisfy the relation $0^\circ < \Phi < 45^\circ$.
- (3) At frequencies in the range $\omega_L < \omega < \omega_{ct}$, we have the activation controlled regime (III) where the phase value $\Phi (< 45^\circ) \rightarrow 0^\circ$. In this regime the charge transfer kinetics of MDR is the limiting process that essentially control the corrosion. The phase value satisfy the relation $45^\circ > \Phi > 0^\circ$ and the slope $\log |Z|$ vs $\log \omega$ is less than $(-1/2)$.
- (4) At frequencies in the range $\omega_{ct} < \omega < \omega_i$, we have the mixed diffusion-kinetic controlled regime (IV) where the slope of $\log |Z|$ vs $\log \omega$ increases from $(1/2)$ to 1 correspondingly the phase value increases towards 90° indicating the coupled contribution of charge transfer kinetics, the steady state diffusion corrosion current and the EDL capacitance. In this regime, there is a competition of the MDR and ORR rates.
- (5) At frequencies in the range $\omega_i < \omega < \omega_\Omega$, the phase rises towards 90° , attains a peak and tends to 0° . This regime shows the switching from capacitive ($\Phi = 90^\circ$) electric double layer to electrolyte Ohmic controlled regime ($\Phi = 0^\circ$).
- (6) At frequencies $\omega > \omega_\Omega$, we have the purely Ohmic controlled regime and the impedance plot shows a constant straight line with slope of $\log |Z|$ vs $\log \omega$ equal to 0 (zero) and the asymptotic value of impedance is equal to resistance of electrolyte R_Ω . In this regime the phase plots shows a value of $\Phi = 0^\circ$.

3.2 Comparison of limiting impedances

To gain insight into the impedance behaviour under various conditions we consider some limiting cases of the general case given by equation 7. Figure 3 shows the comparison of impedance responses in (a) $\log |Z|$ (b) phase Φ , and (c) complex impedance Z' vs Z'' as a function of frequency ω . The line (red) A represent the impedance response of a metal corrosion under an electrolyte layer given by equation 7. The line (blue) B represents the case of constant MDR current density corresponding to a highly active metal surface when the double layer capacitance is ignored or negligible and the system is fully supported. Here $R_{ct} \rightarrow 0$, $C_{dl} \rightarrow 0$ and $R_\Omega \rightarrow 0$. The line (black) C represents the finite length Warburg impedance given by equation 8. The line (green) D represents the impedance of the corroding metal/electrolyte interface where the electrolyte is well supported, i.e., $R_\Omega = 0$. The line (red dashed) E represents the pure classical Warburg impedance obtained from equation 8 when the electrolyte layer thickness is very large i.e., $L \rightarrow \infty$.

The red line in in Nyquist plot in Figure 3(c) shows two arcs with an intervening straight line representing a finite length Warburg type impedance. The low frequency arc corresponds to the diffusion of oxygen in the electrolyte layer film whereas the high frequency arc corresponds to the Faradaic process at the interface. At lower frequency $\omega < \omega_L$, the impedance response merges with the impedance plot (blue line) of corresponding a constant metal dissolution current where both the charge transfer resistance ($R_{ct} \rightarrow 0$) and double layer capacitance ($C_{dl} \rightarrow 0$) are negligible and the system is fully supported i.e., $R_\Omega \rightarrow 0$. At very low frequencies where $\omega < \omega_D$, the impedance arc closes itself asymptotically with the real axis which indicates that the interface is not entirely diffusion controlled or capacitive but a coupled regime of both. The plot is a reminiscent of Cole-Davidson-type lemniscates,⁶³ and may be seen as a ‘‘pseudo depressed’’ arc which arises due to heterogeneous charge transfer reaction, but without inclusion of constant phase element (CPE).

The value of the intercept of the Nyquist curve on the real axis at very low frequency gives the effective resistance of interface and can be analytically derived from equation 13 and is given by equation 14. The intercept in the Nyquist (solid red) curve at high frequency region gives the magnitude of solution resistance of electrolyte R_Ω relative to $Z(\omega \rightarrow 0)$ and is $Z(\omega \rightarrow \infty) \sim R_\Omega$.



◀ **Figure 3.** Different limiting impedance characteristic as predicted by equation 13 in terms of (a) magnitude of impedance, (b) phase, and (c) complex impedance plots as function of frequency ω (radians per second). Here A (red line)- impedance (Z) given by equation 7; B(blue line)- $Z(R_{ct} \rightarrow 0, C_{dl} \rightarrow 0, R_{\Omega} \rightarrow 0)$; C(black line)- finite length Warburg (Z_{FLW}); D(green line)- impedance of corroding system in presence of supporting electrolytes, $Z(R_{\Omega} \rightarrow 0)$; E(dotted red line)- pure classical Warburg impedance. The physical parameters are : $n_2 = 4$, $F = 96500 \text{ C mol}^{-1}$, $T = 293 \text{ K}$, $R = 8.314 \text{ JK}^{-1} \text{ mol}^{-1}$, $C_{st} = 0.24 \text{ mol m}^{-3}$, $i_{st} = 9.6 \text{ Am}^{-2}$, $D = 2.2 \times 10^{-9} \text{ m}^2 \text{ s}^{-1}$, $L = 1.5 \text{ mm}$.

3.3 Effect of electrolyte layer thickness

Figure 4 shows the effect of L on (a) magnitude (b) phase and (c) complex impedance in some limiting cases given by equation 13. At low frequency $\omega < \omega_D$, as L increases the corrosion becomes diffusion controlled and phase $\Phi \rightarrow 45^\circ$ (blue line in Figure 4(b)). A thin layer shows more kinetic resistance controlled with $\Phi \rightarrow 0$ (red line in Figure 4(b)). A transition from diffusion controlled to kinetic resistance controlled can be identified with the hump shape in the phase plot in low frequency (black line in Figure 4(b), $L = 10 \mu\text{m}$). These are typical of electrolyte layer thickness in experiments where maximum corrosion rate is observed, e.g. in iron $L \sim 10 \mu\text{m}^{10}$ and for copper (covered with an acidic solution containing sulphate ions) $L \sim 30-40 \mu\text{m}^{13}$.

In the Nyquist plot Figure 4 (c) (red line) we observe that in thinner electrolyte layer the impedance shows only one arc typical of an RC-equivalent circuit response. The second arc at low frequency shrinks as we reduce the thickness of electrolyte. This suggest that corrosion in very thin electrolyte is more kinetic (Faradaic) controlled.

3.4 Effect of Diffusion Coefficient of Oxygen

The value of diffusion coefficient of dissolved oxygen D , dissolved in electrolyte depends on concentration of salts like NaCl or Na_2SO_4 and the temperature of solution. For example the order of oxygen diffusivities

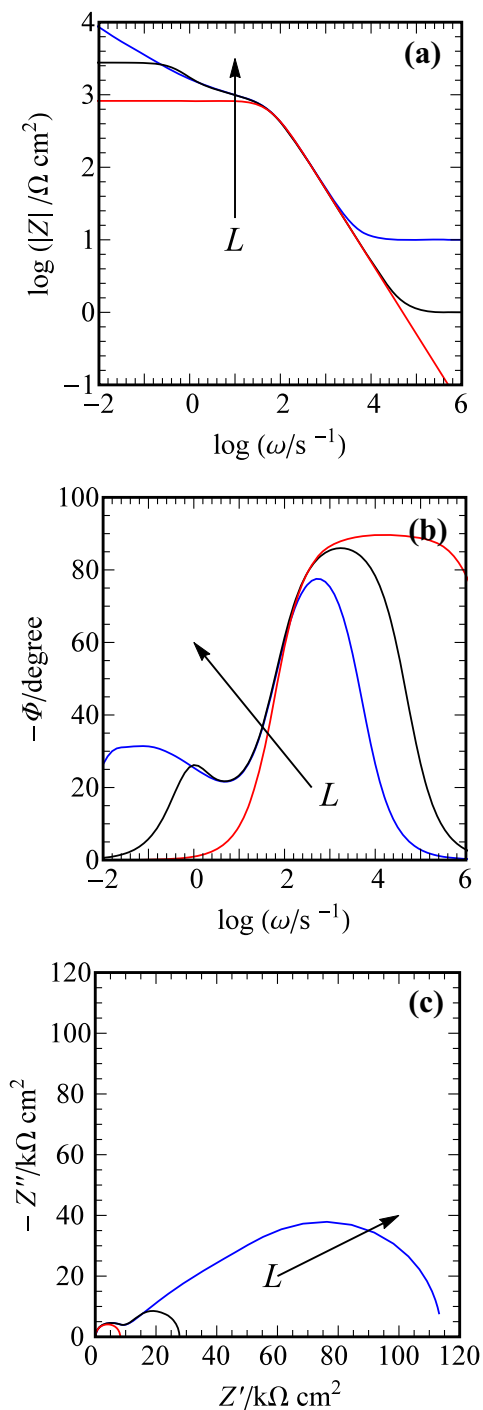


Figure 4. Comparison of various electrolyte thickness dependent limiting impedance of the model in (a) magnitude of impedance, (b) phase and (c) complex impedance plots. The physical parameters are: $n_2 = 4$, $F = 96500 \text{ C mol}^{-1}$, $T = 293 \text{ K}$, $R = 8.314 \text{ J K}^{-1} \text{ mol}^{-1}$, $C_{st} = 0.24 \text{ mol m}^{-3}$, $D = 2.2 \times 10^{-9} \text{ m}^2 \text{ s}^{-1}$, $i_{st} = 2.88 \text{ A m}^{-2}$, $L(\mu\text{m}) = 1$ (red line), 10 (black line), 100 (blue line). Note that the solution resistance is calculated using $R_{\Omega} = \rho(L/A)$ where ρ is the specific resistance of electrolyte, L is the thickness of electrolyte and A is the contact area of electrolyte with metal surface. Here $\rho = 10 \text{ m}\Omega \text{ m}^{-1}$ and $A = 1 \text{ mm}$.

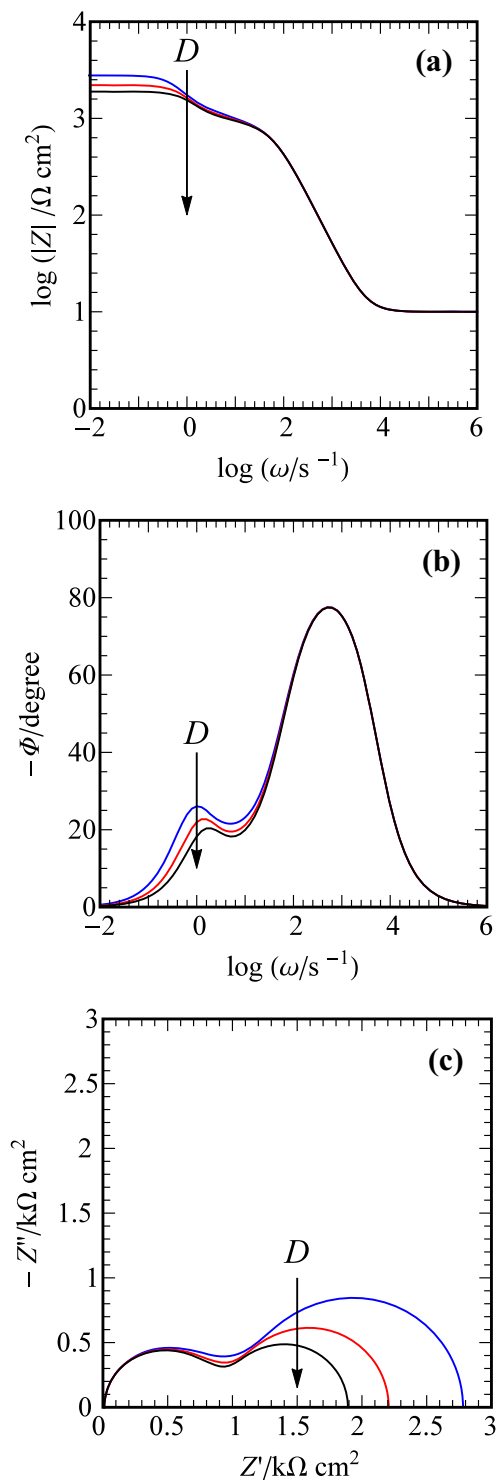


Figure 5. Effect of diffusion coefficient of oxygen on (a) magnitude of impedance, (b) phase and (c) complex impedance. The plots were generated with physical parameters: $C_{dl} = 20 \mu\text{F cm}^{-2}$, $F = 96500 \text{ C mol}^{-1}$, $C_{st} = 0.24 \text{ mol m}^{-3}$, $A = 1 \text{ mm}$, $\rho = 10^{-2} \Omega \text{ m}$, $L = 0.1 \text{ mm}$ and $i_{st} = 2.88 \text{ A m}^{-2}$. Here $D(\text{m}^2 \text{ s}^{-1}) = 2.2 \times 10^{-9}$ (blue line), 3.2×10^{-9} (red line), 4.2×10^{-9} (black line) respectively.

are 2.9×10^{-5} , 3.5×10^{-5} , 4.4×10^{-5} cm^2s^{-1} for platinum electrode in 0.2, 0.1 and 0.05 kmol m^3 Na_2SO_4 ,¹³ respectively. In Figure 5 we observe that change of diffusion coefficient has effect only when $\omega < \omega_i$. The $\log |Z|$ vs $\log \omega$ plot shows that for frequencies $\omega < \omega_D$ the value of $|Z|$ decreases as we increase D . The phase plot in (b) shows a shift in phase-peak towards higher frequencies and simultaneous decrease in phase value indicating that increase in diffusion coefficient speeds up the transition from diffusion to kinetic Faradaic controlled regime. Thus change in D is found to affect both the finite electrolyte layer thickness and Faradaic regime at $\omega_L < \omega < \omega_i$ and results in shrinking of the frequency regime as we increase D .

Figure 5(c) shows that increasing D decreases the size of arc at low frequency because the frequency of onset of diffusion controlled cathodic reduction is shifted to higher value ($\omega_D \propto D$) with a simultaneous decrease in the effective resistance since $Z_{\text{FLW}} \propto 1/D$. However there is no appreciable effect on the size of high frequency arc.

3.5 Effect of steady state ORR current density

Figure 6 shows the effect of steady state ORR current density i_{st} on (a) magnitude (b) phase and (c) complex impedance plots given by equation 3. We observed that i_{st} has a huge effect on the mixed kinetic-diffusion, finite electrolyte thickness and purely diffusion controlled regimes. The electric double layer and the solution Ohmic regimes at frequencies $\omega > \omega_i$ are least affected.

The magnitude of impedance plot (a) show that as we increase i_{st} , both the activation controlled ($\omega_L < \omega < \omega_{\text{ct}}$) and the mixed kinetic-diffusion controlled regions $\omega_{\text{ct}} < \omega < \omega_i$ is mitigated. For large i_{st} the frequencies the regimes *viz.*, diffusion control finite electrolyte layer regime, the activation controlled regime and mixed kinetic-diffusion regimes merge resulting in disappearance of intermediated impedance plateau (black line).

The phase (b) plots show that at low i_{st} the phase has a hump like feature with phase peak $\Phi < 45^\circ$. This feature changes to a step like feature with $\Phi \rightarrow 45^\circ$. The step or hump like phase behavior vanishes at higher values of i_{st} .

The Nyquist plot (c), at low i_{st} (blue line) shows two arcs. The arc in high frequency corresponding to Faradaic process is relatively larger in size than the

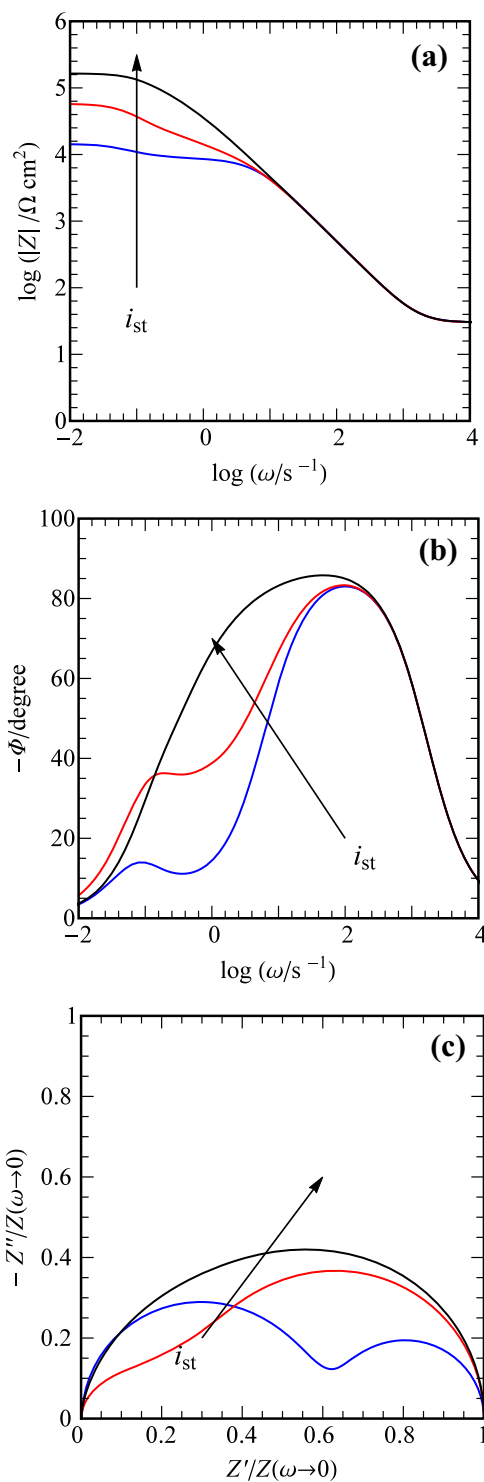


Figure 6. Effect of steady state oxygen reduction reaction current density on (a) magnitude of impedance, (b) phase and (c) complex impedance. The plots were generated with physical parameters: $C_{\text{dl}} = 20 \mu\text{F cm}^{-2}$, $F = 96500 \text{ C mol}^{-1}$, $C_{\text{st}} = 0.24 \text{ mol m}^{-3}$, $D = 2.2 \times 10^{-9} \text{ m}^2 \text{ s}^{-1}$, $A = 1 \text{ mm}$, $\rho = 10^{-3} \Omega \text{ m}$, $L = 0.1 \text{ mm}$ and $i_{\text{st}}(\text{A m}^{-2}) = 0.288$ (blue line), 2.88 (red line), 28.8 (black line).

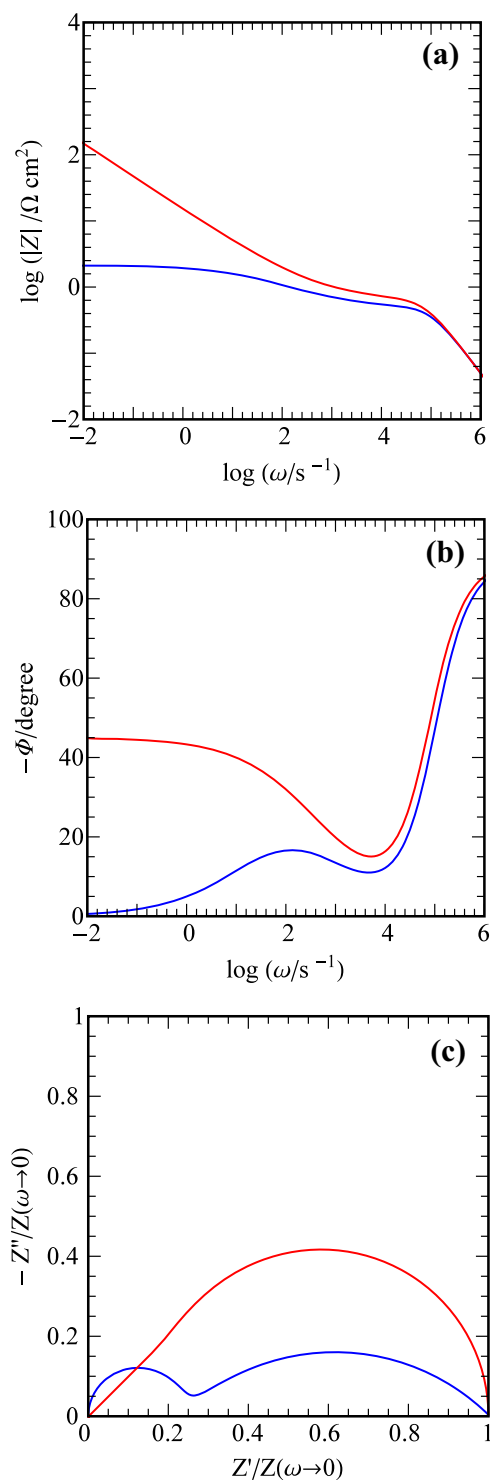


Figure 7. Impedance plots for system with high (red line) and low metal (blue line) dissolution current corresponding to $R_{ct} = 0.214 \text{ m}\Omega \text{ cm}^2$ and $R_{ct} \rightarrow \infty$ respectively. The plots are generated for the following physical parameters: $n_2 = 4$, $\alpha_{O_2/OH^-} = 0.95$, $F = 96500 \text{ C mol}^{-1}$, $T = 293 \text{ K}$, $R = 8.314 \text{ J K}^{-1} \text{ mol}^{-1}$, $C_{st} = 0.24 \text{ mol m}^{-3}$, $D = 2.2 \times 10^{-9} \text{ m}^2 \text{ s}^{-1}$, $i_{st} = 100 \text{ A m}^{-2}$, $R_{\Omega} = 0$, and $L(\mu\text{m}) = 200$.

low frequency one which corresponds to diffusion controlled regime. At higher i_{st} (red line) the diffusion controlled arc in low frequencies becomes larger in size than the Faradiac controlled arc with a small Warburg regime in between the two arcs. However, at very high i_{st} (black line) the two arcs merge indistinguishably into one large slightly skewed arc.

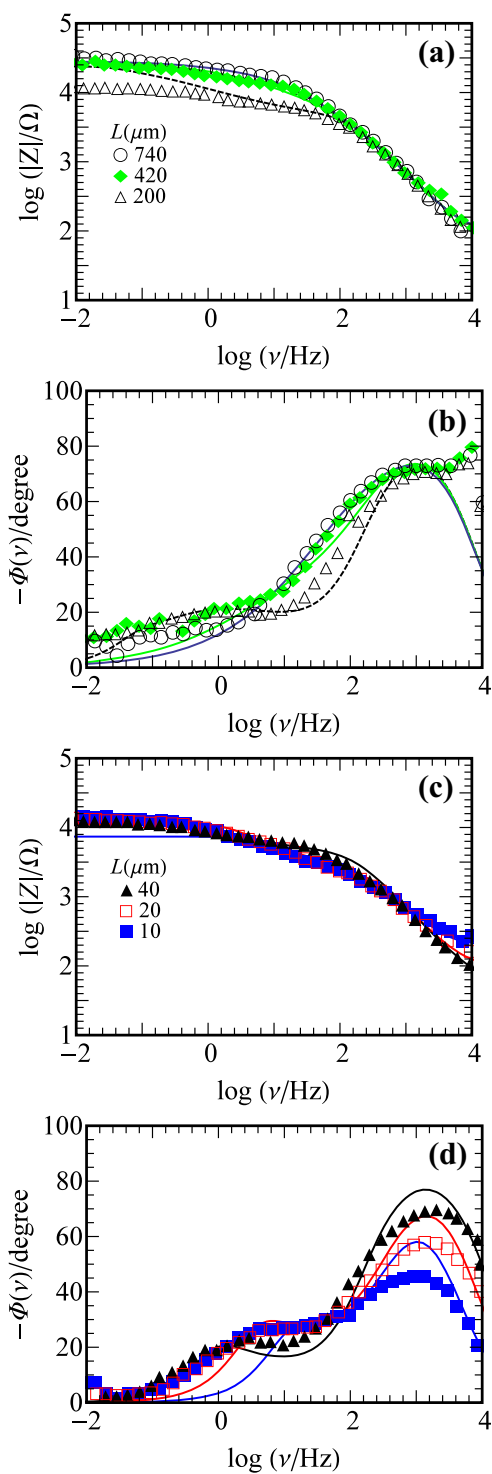
3.6 Effect of MDR Currents

Figure 7 shows the effect of anodic (MDR) rates on the impedance response of corroding metal. The change in MDR affects the Faradaic region where frequencies $\omega < \omega_i$. For a large metal dissolution current density where $R_{ct} < R_D$ (red line), at $\omega < \omega_L$, the corrosion is diffusion controlled as exemplified by the the magnitude of slope of impedance plot approaching (1/2). The phase plot (b) shows an extended Warburg region towards low frequency with $\Phi \rightarrow 45^\circ$ with a broad mixed controlled region in $\omega_L < \omega < \omega_i$. In the Nyquist plot we observe a lemniscate shaped response reminiscent of Cole-Davidson response.^{63,64}

However at low metal dissolution current density where $R_{ct} > R_D$ the impedance (blue line) show a small diffusion controlled regime at frequency $\omega < \omega_L$. The small hump in phase plot with phase peak value much less than 45° shows that the impedance is not purely Warburg controlled but is influence by the Faradiac process. The Nyquist plot (c) (blue line) show a combinations of two arcs. A regular arc is observed at frequency $\omega > \omega_i$ due to coupling of the charge transfer resistance and the electric double layer capacitance and a skewed arc resulting due to the competition between Faradaic charge transfer and the diffusion of oxygen at low frequencies. Similar impedance responses are also observed in supported/ unsupported conditions in electrochemical system consisting electrodes with finite separation.⁵⁴

3.7 Comparison with experiments

Figure 8 shows the comparison of theoretical impedance to the experimental data of copper,¹⁴ covered with a 1 M Na_2SO_4 solution of different electrolyte layer thickness. The data was taken at pH 3 where the corrosion is oxygen diffusion limited (rate determining) coupled with ORR.¹⁴ The parameters used to generate the theoretical plots with corresponding electrolyte layer thickness are listed in Table 1. The



◀ **Figure 8.** Comparison of theory to the experimental data¹⁴ of copper covered with a 1 M Na₂SO₄ solution of pH 3 at different electrolyte layer thickness for a cell dimension length = 1 cm and breadth = 0.01 cm. Here ν is the frequency and $\nu = \omega/2\pi$. The plots were generated using the following parameters: $F = 96485 \text{ C mol}^{-1}$,^{14,16} $D = 2.3 \times 10^{-9} \text{ m}^2 \text{ s}^{-1}$, $C_{dl} = 0.25 \mu\text{F cm}^{-2}$, $n = 2$ with steady state current i_{st} show in Figure 9. In (a) and (b): navy blue line ($L = 740 \mu\text{m}$), green line ($L = 420 \mu\text{m}$) and dotted black line ($L = 200 \mu\text{m}$). In (c) and (d): black line ($L = 40 \mu\text{m}$), red line ($L = 20 \mu\text{m}$) and blue line ($L = 10 \mu\text{m}$).

Table 1. Physical parameters for impedance spectra in Figure 8.

Figure	L (μm)	i_{st} (A m^{-2})	R_{ct}^{-1} ($\Omega^{-1} \text{m}^{-2}$)
8(a) & (b)	740	1	10
	420	1	20
	200	3	25
8(c) & (d)	40	5	35
	20	7	10
	10	15	5

data are for (i) thick electrolyte layer where $L(\mu\text{m}) = 740, 420, 200$ and (ii) thin electrolyte layer with thickness $L(\mu\text{m}) = 40, 20, 10$, respectively. The impedance shows reasonable agreement but deviation from theoretical model predictions are seen. The deviation is larger for thick (Figure 8(a) and (b)) electrolyte layer than for thin electrolyte layer (Figure 8(c) and (d)). The phase plots show more sensitivity to the change in electrolyte layer thickness. The data in agreement with theoretical prediction shows at high frequencies ($\omega_i < \omega < \omega_\Omega$) there is phase peak which results from the competition between Ohmic resistance of the solution and the electric double layer capacitance. However the theoretical phase plots overestimates the magnitude of phase. This is may be due to non inclusion of surface heterogeneity or roughness,^{65,66} pH effects and oxide formation in the process of corrosion. It must be noted that the electrodes prepared in Ref.¹⁴ are heterogeneous in nature due to polishing with 2000 grit SiC paper. It is known

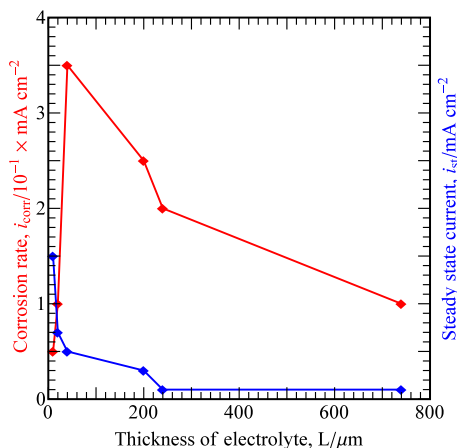


Figure 9. Plots of corrosion current rates and steady state current as a function of electrolyte layer thickness of Figure 8.

that heterogeneity,⁶⁵ and polishing of the electrode surface affect the shape of EIS spectra.^{31,32,66} Here, our model is for a homogeneous surface under uniform corrosion and hence due to non-inclusion of surface heterogeneity the deviations of theoretical curves from the experimental data are seen.

Figure 9 shows plot of corrosion rate and steady state current (obtained from fitting) as a function of thickness of electrolyte i_{corr} is estimated from employing the Stern-Geary equation,^{17,67}

$$i_{\text{corr}} = k/R_{\text{ct}} \quad (15)$$

with $k = 10$ mV and R_{ct} obtained from fitting. The steady state current i_{st} (indicated by blue line) show an exponential fall in current behavior with increase in thickness of electrolyte. The corrosion current (indicated by red line) show a maximum corrosion rate for 40 μm thick electrolyte layer. This is in agreement with earlier experimental studies of diffusion limited current density and electrolyte film thickness (see Figure 7 and 8 in Ref.¹³) where the observation of maximum corrosion rate so called “critical thickness” for copper was found to be approximately 40 μm . Further comparison of experimental impedance data of Pt electrode was made and reasonable agreement was also found (see Figure S2, Supplementary Information).

4. Conclusions

In summary a model for the impedance of atmospheric corrosion of metal in contact with a thin electrolyte layer under pseudo-steady state has been developed. A detailed analysis of influence of thickness of

electrolyte layer, diffusion of oxygen and cathodic and anodic rates has been carried out. The impedance spectra and its frequency response corroding metal in contact with a thin electrolyte layer show the following six regimes: (i) diffusional resistance controlled regime, (ii) electrolyte film thickness controlled, (iii) activation controlled, (iv) mixed diffusion and kinetic controlled, (v) electric double layer regime and (vi) purely Ohmic solution regime. These regimes are characterized by five characteristic frequencies *viz.*, ω_{D} , ω_{L} , ω_{ct} , ω_{i} and ω_{Ω} . The impedance phase characteristics shows the following values associated with the above six regimes: (i) $\Phi = 0^\circ$, (ii) $0^\circ < \Phi \rightarrow 45^\circ$, (iii) $45^\circ > \Phi \rightarrow 0^\circ$, (iv) $0^\circ < \Phi \rightarrow 90^\circ$, (v) $90^\circ > \Phi \rightarrow 0^\circ$, and (vi) $\Phi = 0^\circ$. The model presented here establishes the following points for corrosion of metal in contact with a thin electrolyte layer:

- The initial process of metal corrosion in contact with a thin electrolyte layer is a coupled heterogeneous charge transfer-diffusion system due to competition of the two processes *viz.*, MDR and ORR.
- When the electrolyte film thickness is larger than the diffusion layer thickness, the rate of corrosion is the diffusion-limited. This observation is in agreement with Tomashov model of atmospheric corrosion of metal⁹ whereas for thin electrolyte layer film the rate of corrosion is charge transfer limited.
- Impedance analysis can easily distinguish the onset and the transition from charge transfer to diffusion limited regimes and their identifies the characteristic frequencies.
- The comparison of theory with copper corrosion of data¹³ suggest that maximum corrosion can take place at a critical thickness which induce a change from diffusion controlled to Faradaic control and physically corresponds to moist-wet transition. However, the possible role of the surface morphology of the metal surface cannot be ignored in interpretation of the rates of corrosion.

Finally, the novelty of the model presented lies in the fact that unlike experimental studies employing weight loss methods or Tafel polarization methods, it can help study the initial stages of corrosion in presence of mass transfer effects and determine the rate of corrosion. Also, electrochemical impedance spectroscopy, being a non-invasive experimental technique, it may be used to study corrosion without loss of material. Furthermore experimental studies employing equivalent circuit model without any physical basis, may be

replaced with the theoretical description provided here for corrosion of metal in contact with thin electrolyte layer. The analytical results are derived rigorously solving the pertinent governing equation and the boundary conditions and it provides a clear physical picture of all the process taking place in atmospheric corrosion of metal in contact with a thin electrolyte. The model also identify the multi-regime aspect of corrosion using impedance technique in one study. Furthermore various electrochemical components viz., charge transfer resistance, diffusional resistance, ohmic resistance, EDL capacitance related to physical mechanism, dimensions and conditions pertaining to corroding system can be obtained from the model. However, since atmospheric corrosion of metal under a thin electrolyte film is a complex multi-scale and multi-physics phenomena involving natural convection^{21,22} in the thin electrolyte film, change in pH and surface morphology^{31,32,66,68,69} coupled with a complex multi-step ORR reaction pathway the study of corrosion is far from complete. A proper theoretical study that may account these effects is still lacking. The study of these problems is beyond the scope of present paper and will be presented elsewhere.

Supplementary Information (SI)

Supplementary Information is available at www.ias.ac.in/chemsci.

Acknowledgements

MBS acknowledges the DST, New Delhi, India for the award of DST Inspire Faculty. MBS also acknowledges CSIRO (Australia) where initial part of research was carried out as Visiting Scientist.

Declarations

Conflict of interest The authors declare no competing financial/commercial interest.

References

- Cole I S, Azmat N S, Kanta A and Venkatraman M S 2009 What really controls the atmospheric corrosion of zinc? Effect of marine aerosols on atmospheric corrosion of zinc *Int. Mater. Rev.* **54** 117
- Cole I S, Muster T H, Azmat N S, Venkatraman M S and Cook A 2011 Multiscale modelling of the corrosion of metals under atmospheric corrosion *Electrochim. Acta* **56** 1856
- Gunasegaram D R, Venkatraman M S and Cole I S 2014 Towards multiscale modelling of localised corrosion *Inter. Mat. Rev.* **59** 84
- Simillion H, Dolgikh O, Terryn H and Deconinck J 2014 Atmospheric corrosion modeling *Corr. Rev.* **32** 73
- McCafferty E 2010 *Introduction to Corrosion Science* (Springer: New York) p. 8
- Muster T H, Bradbury A, Trinchi A, Cole I S, Markley T, Lau D, Dligatch S, Bendavid A and Martin P 2011 The atmospheric corrosion of zinc: The effects of salt concentration, droplet size and droplet shape *Electrochim. Acta* **56** 1866
- Leygraf C, Wallinder I.O, Tidblad J and Graedel T 2016 *Atmospheric Corrosion* (Wiley: Hoboken) p. 22
- Schweitzer P A 2007 *Fundamentals of Metallic Corrosion: Atmospheric and Media Corrosion of Metals* (CRC Pres: Taylor and Francis group) p. 39
- Tomashov N D 1964 Development of the electrochemical theory of metallic corrosion *Corros.* **20** 7t
- Stratmann M and Streckel H 1990 On the atmospheric corrosion of metals which are covered with thin electrolyte layers- I. Verification of the experimental technique *Corros. Sci.* **30** 681
- Stratmann M and Streckel H 1990 On the atmospheric corrosion of metals which are covered with thin electrolyte layers- II. Experimental results *Corros. Sci.* **30** 697
- Stratmann M, Streckel H, Kim T and Crockett S 1990 On the atmospheric corrosion of metals which are covered with thin electrolyte layers- III. Measurements of polarization curves on metal surfaces which are covered by thin electrolyte layers *Corros. Sci.* **30** 715
- Tsuru T, Nishikata A and Wang J 1995 Electrochemical studies on corrosion under a water film *Mater. Sci. Eng. A* **198** 161
- Nishikata A, Ichihara Y and Tsuru T 1995 An application of electrochemical impedance spectroscopy to atmospheric corrosion study *Corros. Sci.* **37** 897
- Nishikata A, Ichihara Y and Tsuru T 1996 Electrochemical impedance spectroscopy of metals covered with a thin electrolyte layer *Electrochim. Acta* **41** 1057
- Nishikata A, Ichihara Y, Hayashi Y and Tsuru T 1997 Influence of electrolyte layer thickness and pH on the initial stage of the atmospheric corrosion of iron *J. Electrochem. Soc.* **144** 1244
- Shi Y, Tada E and Atsushi Nishikata A 2015 A method for determining the corrosion rate of a metal under a thin electrolyte film *J. Electrochem. Soc.* **162** C135
- Nishikata A, Yamashita Y, Katayama H, Tsuru T, Usami A, Tanabe K and Mabuchi H 1995 An electrochemical impedance study on atmospheric corrosion of steel in a cyclic wet-dry conditions *Corros. Sci.* **37** 2059
- Chung K W and Kim K B 2000 A study of the effect of concentration build-up of electrolyte on the atmospheric corrosion of carbon steel during drying *Corros. Sci.* **42** 517
- Frankel G S, Stratmann M, Rohwerder M, Michalik A, Maier B, Dora J and Wicinski M 2007 Potential control under thin aqueous layers using a Kelvin Probe 2007 *Corros. Sci.* **49** 2021
- Liu C, Srinivasan J and Kelly R G 2017 Electrolyte film thickness effects on the cathodic current availability in a galvanic couple *J. Electrochem. Soc.* **164** C845
- Katona R M, Carpenter J C, Knight A W, Marshall R S, Nation B L, Schindelholz E J, Schaller R F and Kelly R

- G 2021 Natural convection boundary layer thickness at elevated chloride concentrations and temperatures and the effects on a galvanic couple *J. Electrochem. Soc.* **168** 031512
23. Zhang S H and Lyon S B 1994 Anodic process on iron covered by thin dilute electrolyte layer (II) A. C. impedance measurements *Corros. Sci.* **36** 1309
 24. Zhang T, Chen C, Shao Y, Meng G, Wang F, Li X and Dong C 2008 Corrosion of pure magnesium under thin electrolyte layers *Electrochim. Acta* **53** 7921
 25. Liao X, Cao F, Zheng L, Liu W, Chen A, Zhang J and Cao C 2011 Corrosion behaviour of copper under chloride-containing thin electrolyte layer *Corros. Sci.* **53** 3289
 26. Liu W, Cao F, Chen A, Chang L, Zhang J and Cao C 2010 Corrosion behaviour of AM60 magnesium alloys containing Ce or La under thin electrolyte layers. Part 1: Microstructural characterization and electrochemical behaviour *Corros. Sci.* **52** 627
 27. Cheng Y L, Zhang Z, Cao F H, Li J F, Zhang J Q, Wang J M and Cao C N 2004 A study of the corrosion of aluminum alloy 2024-T3 under thin electrolyte layers *Corros. Sci.* **46** 1649
 28. Xing S, Li Y, Wu J and Yan Y 2010 Electrochemical methods study on corrosion of 5% Al-Zn alloy-coated steel under thin electrolyte layers *Mater. Corros.* **61** 428
 29. Xiao K, Dong C F, Luo H, Lui Q and Li X G 2012 Investigation on the electrochemical behaviour of copper under HSO_3^- containing thin electrolyte layers *Int. J. Electrochem. Sci.* **7** 7503
 30. Huang H, Guo X, Zhang G and Dong Z 2011 Effect of direct current electric field on atmospheric corrosion behaviour of copper under thin electrolyte layer *Corros. Sci.* **53** 3446
 31. Ingelgem Y V, Hubin A and Vereecken J 2008 Application of multisine impedance spectroscopy, FE-AES and FE-SEM to study the early stages of copper corrosion *Electrochim. Acta* **53** 7523
 32. Ingelgem Y V, Tourwe E, Vereecken J and Hubin A 2008 Application of multisine impedance spectroscopy, FE-AES and FE-SEM to study the early stages of copper corrosion *Electrochim. Acta* **53** 7523
 33. El-Feki A A, Broadbridge P and Walter G W 1999 Exact solutions of potentiostatic current transients for a corrosion reaction under mixed charge transfer and diffusion control *Math. Comput. Modell.* **29** 27
 34. El-Feki A A, Broadbridge P and Walter G W 1999 Potential Transients for an electrochemical corrosion reaction under constant current conditions *Math. Comput. Modell.* **30** 111
 35. Cruz R P V, Nishikata A and Tsuru T 1998 Pitting corrosion mechanism of stainless steels under wet-dry exposure in chloride-containing environment *Corros. Sci.* **40** 125
 36. den Steen N V, Simillion H, Dolgikh O, Terryn H and Deconinck J 2016 An integrated modeling approach for atmospheric corrosion in presence of a varying electrolyte film *Electrochim. Acta* **187** 714
 37. Venkatraman M S, Cole I S and Emmanuel B 2011 Model for corrosion of metals covered with thin electrolyte layers: Pseudo-steady state diffusion of oxygen *Electrochim. Acta* **56** 7171
 38. Venkatraman M S, Cole I S and Emmanuel B 2011 Corrosion under a porous layer: A porous electrode model and its implications for self-repair *Electrochim. Acta* **56** 8192
 39. Gabriel I B, Venkatraman M S, Cole I S, Moorthy C G and Emmanuel B 2011 Metallic corrosion under a thin electrolyte layer controlled by oxygen diffusion: depressed nyquist arcs without the constant phase element, *CSIRO e-publication*, Manuscript/Document Number EP106760
 40. Gabriel I B, Venkatraman M S, Cole I S and Emmanuel B (2011) Model for corrosion of metals covered with thin electrolyte layers: Pseudo-steady state diffusion of oxygen *Electrochim. Acta* **56** 7171
 41. Venkatraman M S, Bosco I G, Cole I S and Emmanuel B 2011 Models for corrosion of metals under thin electrolyte layers *ECS Trans.* **35** 1
 42. Dolgikh O, Bastos AC, Oliveira A, Dan C and Deconinck J 2016 Influence of the electrolyte film thickness and NaCl concentration on the oxygen reduction current on platinum *Corros. Sci.* **102** 338
 43. Simillion H, den Steen N V, Terryn H and Deconinck J 2016 Geometry influence on corrosion in dynamic thin film electrolytes *Electrochim. Acta* **209** 149
 44. Thebault F, Vuillemina B, Oltra R, Ogle K and Allely C 2008 Investigation of self-healing mechanism on galvanized steels cut edges by coupling SVET and numerical modeling *Electrochim. Acta* **53** 5226
 45. Thebault F, Vuillemin B, Oltra R, Allely C and Ogle K 2011 Modeling bimetallic corrosion under thin electrolyte films *Corros. Sci.* **53** 201
 46. Koushik B G, den Steen N V, Mamme M H, Van Ingelgem Y and Terryn H 2021 Review on modelling of corrosion under droplet electrolyte for predicting atmospheric corrosion rate *J. Mater. Sci. Tech.* **62** 254
 47. Saedikhani M and Blackwood D J 2020 Finite element method for thin film corrosion modelling: Where we advanced and where we would like to advance? *Corros. Mater. Degrad.* **1** 273
 48. Cole I S 2017 Recent progress and required developments in atmospheric corrosion of galvanized steel and zinc *Materials* **10** 1288
 49. Oldham K B and Myland J C 1994 *Fundamentals of Electrochemical Science* (Academic Press Inc., San Diego, CA) p. 175
 50. Smith J M, Ness H C V and Abbott M 2017 *Introduction to Chemical Engineering Thermodynamics* (McGraw-Hill Companies) p. 614
 51. Garcia H E and Gordon L I 1992 Oxygen solubility in seawater: Better fitting equations *Limnol. Oceanogr.* **37** 1307
 52. Bard A J and Faulkner L R 2001 *Electrochemical Methods, Fundamentals and Applications* (Wiley) p. 99
 53. Calvo E J 2014 The kinetics of oxygen electroreduction: A long way from iron rust to lithium-air batteries *Mater. Corr.* **65** 4

54. Franceschetti D R, Macdonald J R and Buck R P 1991 Interpretation of Finite-Length-Warburg-Type Impedances in Supported and Unsupported Electrochemical Cells with Kinetically Reversible Electrodes *J. Electrochem. Soc.* **138** 368
55. Barsoukov E and Macdonald J R 2018 *Impedance Spectroscopy Theory, Experiment, and Applications* (John Wiley & Sons, Inc) pp. 57–70
56. Lasia A *Electrochemical Impedance Spectroscopy and its Applications* (Springer) p. 88
57. Randles J E B 1947 Kinetics of rapid electrode reactions *Disc. Faraday Soc.* **1** 11
58. Kant R and Singh M B 2015 Generalization of Randles-Ershler admittance for an arbitrary topography electrode: application to random nite fractal roughness *Electrochim. Acta* **163** 310
59. Oragem M E and Tribollet B 2008 *Electrochemical Impedance Spectroscopy* (John Wiley and Sons, Inc.) p. 333
60. Warburg E 1899 Ueber das verhalten sogenannter unpolarisierbarer elektro-den gegen wechselstrom *Ann. Phys. Chem. (Ser. 3)* **67** 493
61. Warburg E 1901 Uber die Polarizationscapacitat des Platins *Ann. Phys. (Leipzig)* **6** 125
62. Nagy Z, Hernes P J, Minkoff M, Leaf G F and and R H 1989 Effect of Diffusion Layer Structure on the Determination of Corrosion Rates from DC Transient Measurements *J. Electrochem. Soc.* **136** 2816
63. Bosco E 2008 Constant phase elements, depressed arcs and analytic continuation: A critique *J. Electroanal. Chem.* **624** 14
64. Bisquert J, Belmonte G G, Santiago F F and Bueno P R 1999 Theoretical models for ac impedance of finite diffusion layers exhibiting low frequency dispersion *J. Electroanal. Chem.* **475** 152
65. Singh M B and Kant R 2011 Debye-Falkenhagen dynamics of electric double layer in presence of electrode heterogeneities *J. Electroanal. Chem.* **704** 197
66. Singh M B and Kant R 2014 Theory of anomalous dynamics of electric double layer at heterogeneous and rough electrodes *J. Phys. Chem. C* **118** 5122
67. Stern M and Geary A L 1957 Electrochemical polarization I. A theoretical analysis of the shape of polarization curves *J. Electrochem. Soc.* **104** 56
68. Toloei A, Stoilov V and Northwood D O 2015 *WIT Transactions on Engineering Sciences C A Brebbia* (Ed.) **90** p 355
69. Bassach P, Quintana G, Ferrer I and Ciurana J 2012 Studying the relation between corrosion and surface roughness *AIP Conf. Proc.* **1431** 319